NURETH14-231

SENSITIVITY ANALYSIS OF HEATED WALL TEMPERATURE AND VELOCITY DISTRIBUTION IN CFD SIMULATIONS OF THE UPWARD FLOW OF SUPERCRITICAL WATER

M. Jaromin and H. Anglart

Royal Institute of Technology (KTH), Stockholm, Sweden jaromin@kth.se, henryk@kth.se

Abstract

The main objective of this work was to investigate sensitivities of the heated wall temperature and radial velocity distribution predictions on selected model parameters, in water flow under supercritical conditions. The study was focused on cases in which deterioration of heat transfer occurs. Numerical simulations of the turbulent, upward flow in a circular tube were performed using the commercial CFD code ANSYS CFX 12.1. Implementation of water properties was according to IAPWS IF97. The model sensitivities were examined on the mesh discretization, boundary conditions and numerical parameters. Results of simulations were compared with the available experimental data.

A significant sensitivity was recognized especially for changes of heat flux and mass flux. It was found out that the model is much less sensitive to changes of boundary conditions for high values of mass flux and heat flux than for low mass and heat fluxes.

Introduction

Supercritical Water Reactor (SCWR) is one of the proposed designs for Gen IV innovative nuclear energy systems. The interest in the SCWR results from opportunities for electricity generation at low cost, realization of the core in fast neutron spectrum, a high conversion ratio, elimination of dryout, potential of waste transmutation, and hydrogen production. From the thermal-hydraulics point of view, the challenge to be met is correct evaluation of the thermal performance and the temperature distribution in the reactor core in case of strong variations of coolant's properties in the vicinity of the pseudo-critical temperature. Investigations of supercritical water thermal-hydraulics are performed within the FP7 EC Collaborative Project THINS.

Above the critical point ($T_c = 647.096 \, K$, $p_c = 22.06 MPa$ for water), the boundary between liquid and gas phases disappears. Thermal-hydraulic behaviour is characterized by strong variations of the thermal-physical properties. The molecular Prandtl number reaches value larger than unity what means that momentum diffuses much quicker compared to heat. Figure 1 shows how density, dynamic viscosity, specific heat and thermal conductivity change with temperature for different values of pressure. For supercritical water, density and thermal conductivity are relatively high, reaching liquid-like values. Whereas viscosity is of the same order as for the gas phase [7]. Specific heat can rise one or even two orders of magnitude higher than values typical for the liquid phase. The temperature for which specific heat reaches the maximum is called the pseudo-critical temperature, $T_{pc} = 651.8 \, K$ at $23.3 \, MPa$ and $T_{pc} = 659.8 \, K$ at $25.5 \, MPa$. In the vicinity of the

pseudo-critical temperature, properties vary especially strongly with slight changes in pressure and temperature [1].

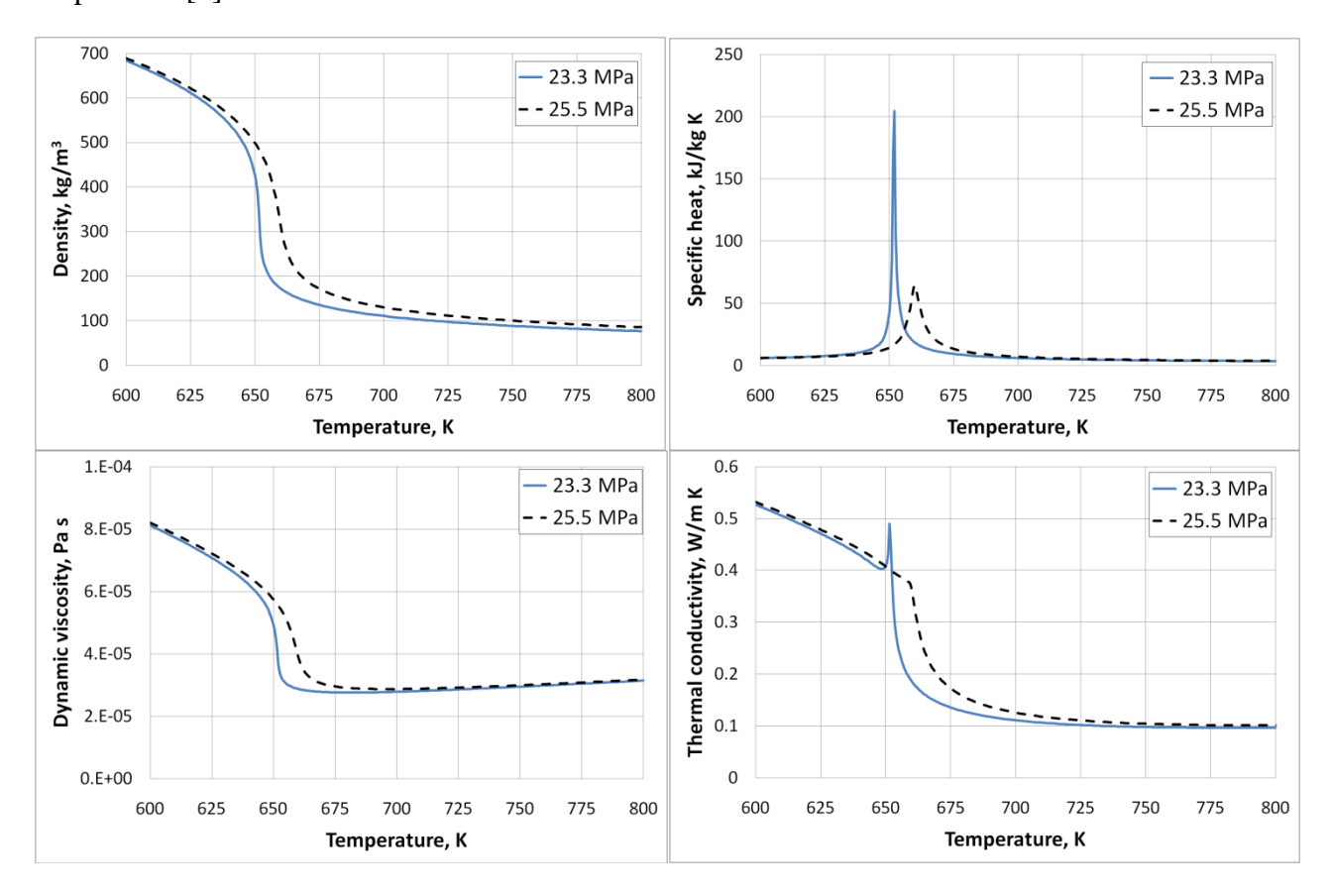


Figure 1 Variations of the thermal-physical properties for water at pressures 23.3 and 25.5 MPa.

The significant changes in properties influence heat transfer to supercritical water. At critical and supercritical pressures, the following heat transfer modes have been recognized: normal, improved and deteriorated [8]. Normal heat transfer is similar to the subcritical fluid where the heat transfer coefficient (HTC) can be calculated with high accuracy using the Dittus-Boelter correlation [11]. Improved heat transfer is characterized by a local rise of the HTC leading to a reduction of wall temperature. Deteriorated heat transfer is characterized by reduction of the HTC in some parts of a test section leading to a rise of wall temperature. The process of heat transfer deterioration occurs gradually, in a narrow range of parameters, and it is not as dramatic as in the case of dryout in two-phase boiling flows [12]. However, since it results in a significant increase of fuel cladding temperature, investigation of this phenomenon is important for defining the safety margins for a SCWR core design. Generally, the enhanced heat transfer can occur for low values of heat flux, and heat transfer is deteriorated or oscillated when the heat flux is high [2]. In this paper, cases with deteriorated heat transfer to supercritical water are investigated.

Heat transfer deterioration has been studied in a number of publications [1,3,5,12-15]. Appearance and magnitude of deterioration is mainly affected by mass flux and heat flux [13]. Koshizuka et al. [1] explain that deterioration occurs due to two mechanisms depending on the flow rate. For large flow rates, heat transfer reduction occurs due to thickening of the viscous sublayer and decrease of

the Prandtl number. For small flow rates, buoyancy force plays an important role by flattening of the velocity profile and therefore reducing the turbulence energy generation.

The onset of heat transfer deterioration is difficult to be defined because the reduction in heat transfer coefficient (thus increase in the wall temperature) proceeds smoothly compare with e.g. the boiling crisis [1]. There are different definitions of the onset of heat transfer deterioration in the literature [3,16-22]. McEligot and Jackson [3] observed that the deterioration of turbulent convective heat transfer in supercritical fluid flow can occur due to radial property variation, acceleration, buoyancy or combination of the phenomena. They discuss parameters which can indicate if any of the mentioned phenomena play a role in a specific case. Impact of the fluid property variation can be determined by calculating the ratios of T_w/T_b or μ_w/μ_b or c_{p_w}/c_{p_b} and also by the non-dimensional heat flux q^+ . Effect of the streamwise acceleration can be measured by the acceleration parameter Kv and the acceleration threshold parameter Ac. From the buoyancy parameter Bo, the onset of buoyancy influences can be determined [3].

The majority of experimental and numerical studies of water at supercritical conditions were performed for circular tubes [12].

1. Modelling approach

The commercial CFD code ANSYS CFX 12.1 is used to simulate the heat transfer to water under supercritical conditions. The flow is turbulent, through a circular tube of small diameter, in an upward direction. The capability of the CFX model will be analyzed by comparing the simulation results with experimental data.

1.1 Governing equations

Governing equations in the steady-state are the continuity, momentum and energy equations, the transport equations of the turbulent kinetic energy and specific dissipation rate in 3 dimensions.

The continuity equation is expressed as [4]:

$$\frac{\partial \rho}{\partial t} + \nabla \cdot (\rho \mathbf{U}) = 0 \tag{1}$$

where ρ is density of fluid and \boldsymbol{U} is a velocity vector. The momentum equation is calculated in the following form [4]:

$$\frac{\partial(\rho \mathbf{U})}{\partial t} + \nabla \cdot (\rho \mathbf{U} \times \mathbf{U}) = -\nabla p + \nabla \cdot \tau + S_{M,buoy}$$
 (2)

where p is the static pressure, τ is a stress tensor related to the strain rate, and $S_{M,buoy}$ is the buoyant production source term [4].

$$\tau = \mu \left(\nabla \boldsymbol{U} + (\nabla \boldsymbol{U})^T - \frac{2}{3} \delta \nabla \cdot \boldsymbol{U} \right) \tag{3}$$

$$S_{M,buoy} = (\rho - \rho_{ref})g \tag{4}$$

The energy equation is expressed as follows [4]:

$$\frac{\partial(\rho h_{tot})}{\partial t} - \frac{\partial \rho}{\partial t} + \nabla \cdot (\rho \boldsymbol{U} h_{tot}) = \nabla \cdot (\lambda \nabla T) + \nabla \cdot (\boldsymbol{U} \cdot \tau) + S_E$$
 (5)

where λ represents thermal conductivity, $\nabla \cdot (\boldsymbol{U} \cdot \tau)$ is a term representing the work due to viscous stresses, S_E is the energy source term, h_{tot} is the total enthalpy, related to the static enthalpy by [4]:

$$h_{tot} = h + \frac{1}{2} \boldsymbol{U}^2. \tag{6}$$

For the modelling of turbulence, the shear stress transport (SST) $k-\omega$ model was selected. This model has been tested and recommended by Palko and Anglart [5] as fully capable of modelling the heat transfer to supercritical water, including the deteriorated region. The SST $k-\omega$ model includes two transport equations to represent the turbulent properties of the flow. The first transported variable is turbulent kinetic energy k and the second variable is the turbulent frequency ω . Generally, two-equation models provide good compromise between the robustness, numerical cost and computational accuracy [4]. One of the advantages of $k-\omega$ model is that it is superior both in its treatment of the viscous near-wall region, and in its accounting for the effects of streamwise pressure gradients [6]. Moreover, $k-\omega$ models do not involve the complex damping function as in $k-\varepsilon$ models and are therefore considered to be more accurate. The two transport equations are solved in CFX in the following form [4]:

$$\frac{\partial(\rho k)}{\partial t} + \frac{\partial}{\partial x_j} \left(\rho U_j k \right) = \frac{\partial}{\partial x_j} \left[\left(\mu + \frac{\mu_t}{\sigma_k} \right) \frac{\partial k}{\partial x_j} \right] + P_k - \beta' \rho k \omega + P_{kb}$$
 (7)

$$\frac{\partial(\rho\omega)}{\partial t} + \frac{\partial}{\partial x_j} \left(\rho U_j \omega \right) = \frac{\partial}{\partial x_j} \left[\left(\mu + \frac{\mu_t}{\sigma_\omega} \right) \frac{\partial \omega}{\partial x_j} \right] + (1 - F_1) 2\rho \frac{1}{\sigma_{\omega 2} \omega} \frac{\partial k}{\partial x_j} \frac{\partial \omega}{\partial x_j} + \alpha \frac{\omega}{k} P_k - \beta \rho \omega^2 + P_{\omega b}$$
 (8)

where ρ is density, μ is dynamic viscosity, k is the turbulent kinetic energy, ω is the turbulent frequency, P_k is the pruduction rate of turbulence, P_{kb} and $P_{\omega b}$ are buoyancy turbulence terms, and α , β' , β , σ_k , σ_{ω} , $\sigma_{\omega 2}$ are the model constants.

To obtain proper transport behaviour, the eddy viscosity is formulated as [4]:

$$\mu_t = \nu_t \rho \tag{9}$$

$$\nu_t = \frac{a_1 k}{\max(a_1 \omega, SF_2)} \tag{10}$$

where S is an invariant measure of the strain rate. Formulation of blending functions F_1 and F_2 is based on a distance to the nearest surface and on flow variables [4]:

$$F_1 = \tanh\left(arg_1^4\right) \tag{11}$$

$$arg_1 = min\left(max\left(\frac{\sqrt{k}}{\beta'\omega y}, \frac{500\nu}{y^2\omega}\right), \frac{4\rho k}{CD_{k\omega}\sigma_{\omega 2}y^2}\right)$$
 (12)

where γ is the distance to the nearest wall, ν is the kinematic viscosity and:

$$CD_{k\omega} = max \left(2\rho \frac{1}{\sigma_{\omega_2}\omega} \frac{\partial k}{\partial x_i} \frac{\partial \omega}{\partial x_i}, 1 \cdot 10^{-10} \right)$$
 (13)

$$F_2 = \tanh\left(arg_2^2\right) \tag{14}$$

$$arg_2 = max\left(\frac{2\sqrt{k}}{\beta'\omega y}, \frac{500\nu}{y^2\omega}\right). \tag{15}$$

Close to walls the blending function is zero, leading to the standard ω equation. Remote from the walls the blending function is equal to unity, corresponding to the standard ε (turbulence eddy dissipation) equation [6].

1.2 Near-wall treatment

The $k-\omega$ turbulence models are recommended for flows requiring high near-wall resolution. The near-wall treatment developed by CFX in the $k-\omega$ models allows for a smooth shift from low-Reynolds number formulation to a wall function formulation. For the momentum equation, an added flux is specified in the following form [4]:

$$F_U = -\rho u^* u_{\tau} \tag{16}$$

where:

$$u^* = \sqrt[4]{\left(\sqrt{\frac{\mu}{\rho} \left|\frac{\Delta U}{\Delta y}\right|}\right)^4 + \left(\sqrt{a_1 k}\right)^4} \tag{17}$$

and u_{τ} is the reference velocity, specified to be used in the law of the wall. u_{τ} is a combination of reference velocities in the viscous sublayer u_{τ}^{vis} and in the logarithmic region u_{τ}^{log} [4].

$$u_{\tau} = \sqrt[4]{(u_{\tau}^{vis})^4 + (u_{\tau}^{log})^4} = \sqrt[4]{\left(\sqrt{\frac{\mu}{\rho} \left|\frac{\Delta U}{\Delta y}\right|}\right)^4 + \left(\frac{U}{1/\kappa \log(y^+) + C}\right)^4}$$
(18)

In the ω -equation, the specific dissipation rate ω_{ω} is blended between the analytical expression for the logarithmic region ω_l and the expression ω_s in the sublayer in the following way [4]:

$$\omega_{\omega} = \omega_s \sqrt{1 + \left(\frac{\omega_l}{\omega_s}\right)^2} \tag{19}$$

where the analytical expression for the logarithmic region is expressed as follows:

$$\omega_l = \frac{u^*}{a_1 \kappa y} = \frac{1}{a_1 \kappa \nu} \frac{u^{*2}}{y^+} \tag{20}$$

and the expression in the sublayer is defined as:

$$\omega_{S} = \frac{6\nu}{\beta(\Delta y)^{2}} \tag{21}$$

with Δy being the distance between the first and the second mesh point. For accurate simulations of heat transfer prediction, fine grid is recommended with $y^+ < 1$.

1.3 Fluid properties

The state-of-the art formulation for the thermodynamic properties of water is IAPWS-95 [24]. It is recommended by the International Association for the Properties of Water and Steam for most applications, especially for scientific use. IAPWS-IF97 is a formulation of water and steam properties prepared for the industrial use where formulations need to be designed for fast and complex computations. IAPWS-IF97 is divided into 5 separate regions, small discontinuities may occur at the region boundaries [23].

The difference between the industrial formulation IAPWS-IF97 and the IAPWS-95 formulation is negligible for most purposes. However, it becomes significant in the very near vicinity of the critical point and in the meta-stable supercooled liquid. Figure 2 shows the difference between the two formulations for selected properties at pressure 23.3 *MPa*.

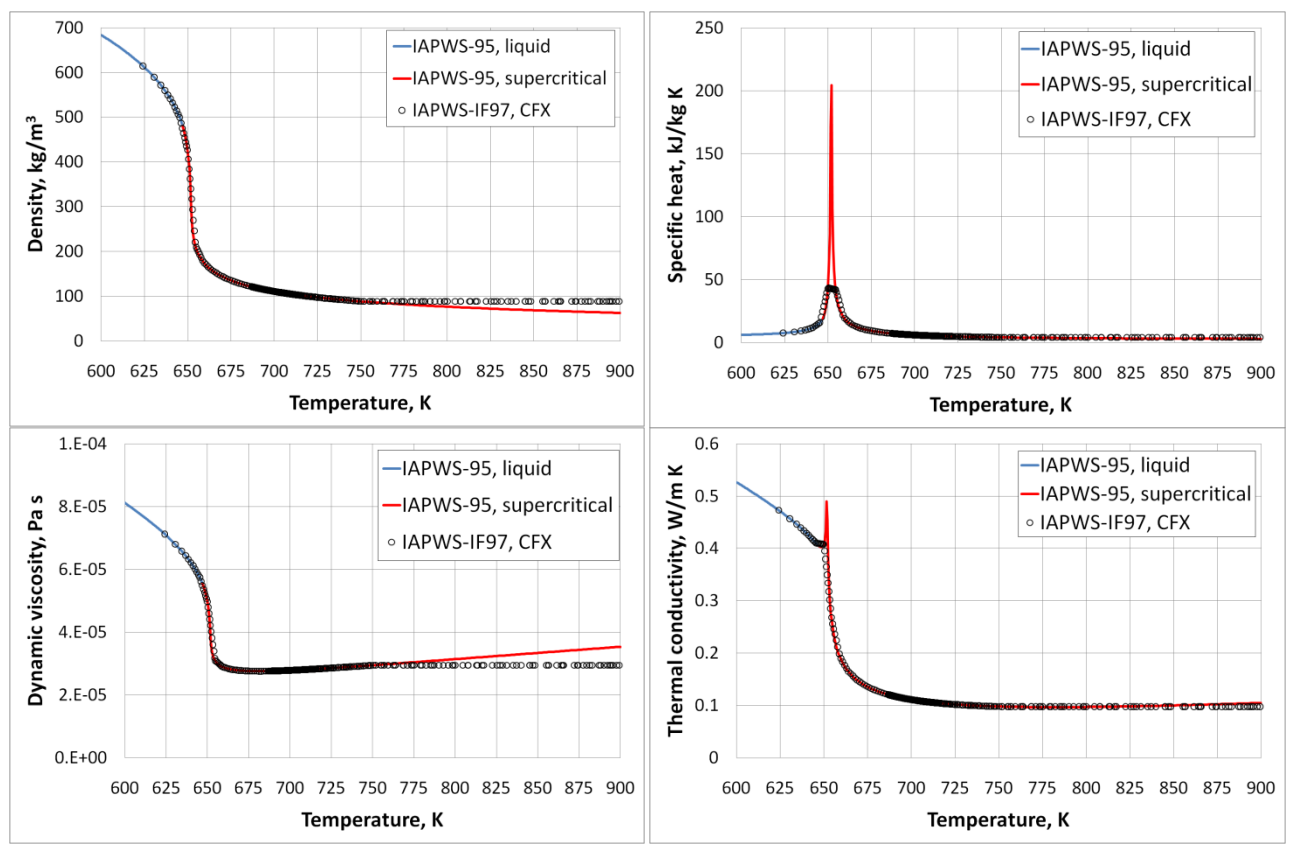


Figure 2 The difference between the industrial formulation IAPWS-IF97 implemented in CFX and the IAPWS-95 formulation, at pressure 23.3 MPa.

In the CFD code ANSYS CFX 12.1, implementation of water properties used in the numerical simulations was according to IAPWS IF97.

Water properties are considered to be only a function of temperature. The impact of pressure on water properties is assumed to be negligible since the pressure change in the pipe is small compared to the absolute pressure.

1.4 Experiments and correlations

An important aspect of numerical simulations is verification of the results against experimental data. In this study, two different experiments were simulated, Shitsman-8 [25] and Ornatskii-359 [26]. Both are characterized by heat transfer deterioration. The experiment by Shitsman [25] was performed at relatively low mass and heat fluxes, while the experiment by Ornatskii [26] was performed at high mass and heat fluxes. Boundary conditions for the simulated experiments are given in Table 1.

	System	Inlet	Mass	Heat	Pipe	Pipe	Pipe
Experiment	pressure	enthalpy	flux	flux	diameter	length	orientation
	MPa	kJ/kg	$kg/(m^2s)$	kW/m ²	mm	m	-
Shitsman-8	23.3	1467.61	430.0	319.87	8.0	1.50	vertical
Ornatskii-359	25.5	662.05	1500.0	1810.00	3.0	0.75	vertical

Table 1 Boundary conditions for simulated experiments.

Simulations were also compared to selected empirical correlations for the Nusselt number. In this study, Bishop, Jackson and Swenson correlations were selected. They were verified for heat transfer into supercritical water in circular tubes. Dittus-Boelter correlation is also chosen for comparison, since most of the empirical correlations have the general form of Dittus-Boelter equation (Eq. 22).

The Dittus-Boelter correlation (Eq. 22) is used for prediction of the convective heat transfer for pure forced convection in turbulent, internal flows through a long, uninterrupted duct at constant, averaged fluid properties [11].

$$Nu = 0.023Re_h^{0.8}Pr_h^{0.4} (22)$$

The real HTC deviates from the Dittus-Boelter correlation especially near the pseudo-critical temperature. It was observed that at low heat fluxes HTC is higher than the Dittus-Boelter prediction. This is called heat transfer enhancement. At high heat fluxes, HTC is lower than from the correlation and under specific conditions can lead to heat transfer deterioration [1].

Bishop correlation (Eq. 23) is applicable for the following ranges of parameters: pressures 22.6-27.5 MPa, mass fluxes $0.68-3.6 \text{ Mg/(m}^2\text{s})$, heat fluxes $0.31-3.5 \text{ MW/m}^2$ and diameters 2.5-5.1 mm [27].

$$Nu_b = 0.0069 \cdot Re_b^{0.9} (Pr_b)^{0.66} \left(\frac{\overline{Cp}}{Cp}\right)^{0.66} \left(\frac{\rho_w}{\rho_b}\right)^{0.43} \left(1 + 2.4 \frac{d}{x}\right)$$
 (23)

In Eq. 23, the last term represents the inlet effect where x is the axial location along the heated length. $\overline{C_P}$ is the average heat capacity defined as:

$$\overline{C_P} = \frac{h_w - h_b}{T_w - T_b}. (24)$$

Jackson correlation is derived in the following form [9-10]:

$$Nu_b = 0.0183 \cdot Re_b^{0.82} (Pr_b)^{0.5} \left(\frac{\overline{c_P}}{c_{Ph}}\right)^n \left(\frac{\rho_W}{\rho_h}\right)^{0.3}$$
 (25)

where the exponent n, in the case of $T_b < T_{ps} < T_w$, is given as:

$$n = 0.4 + 0.2 \left(\frac{T_w}{T_{pc}} - 1 \right). \tag{26}$$

Swenson correlation (Eq. 27) is applicable for the following ranges of parameters: pressures 22.7-41.3 MPa, mass fluxes 0.2-2.0 Mg/(m²s), heat fluxes 0.2-2.0 MW/m² and diameter 9.4 mm. [28]

$$Nu_{w} = 0.00459 \cdot Re_{w}^{0.923} (Pr_{w})^{0.613} \left(\frac{\overline{c_{P}}}{c_{P}}\right)^{0.613} \left(\frac{\rho_{w}}{\rho_{b}}\right)^{0.23}$$
(27)

The bulk temperature T_b is a reference temperature used to calculate the thermal-physical properties in the Dittus-Boelter, Bishop and Jackson correlations. In Swenson correlation, the wall temperature T_w is used to calculate the thermal-physical properties.

1.5 Discretization and boundary conditions

The geometries used in CFD simulations are vertical pipes. Dimensions of the test sections are given in the Table 1. For Shitsman-8, the simulated geometry fully corresponds to the experiment. For Ornatskii-359, extra length of 15 cm was added to the inlet for development of a proper temperature profile in the pipe. A uniform heat flux is specified at walls. The water inlet is placed at the bottom of the pipe. The inlet velocity profile is given as a fully developed turbulent flow, which was obtained from the preliminary calculations in an unheated pipe. The inlet temperature profile is set uniform and turbulence is specified with the intensity of 5%. The outlet is defined as a pressure boundary where the static pressure is specified.

Generated numerical grid is axi-symmetric two-dimensional, composed of hexagonal elements. In the axial direction, grid is uniformly distributed with the cell size equal to 3 mm. In the radial direction, grid distribution is non-uniform. The grid is refined near the heated wall to obtain the non-dimensional length y⁺ lower than 1, and it expands towards the centre of the pipe. Size of the first near-wall cell is 0.001 mm for Shitsman-8 and 0.0015 mm for Ornatskii-359.

2. Computed results

ANSYS CFX 12.1 was used to simulate water flow through a circular, heated tube of small diameter in the upward direction. The flow was fully turbulent and fluid was at supercritical pressure. Steady state conditions are considered. Since the inlet temperature profile is set uniform, the wall surface temperature is low and the heat transfer coefficient is high near the inlet. This region is removed from the calculation results.

Figure 3 shows the axial temperature distribution as a function of bulk enthalpy for both experiments Shitsman-8 and Ornatskii-359. For Shitsman-8, temperature at the inlet is very high, therefore wall temperature reaches the pseudo-critical value in a close vicinity of the inlet. Significant increase in wall temperature was measured in two locations, close to the inlet and in the middle of the pipe. Numerical simulation captures both peaks in the axial temperature distribution (see Figure 3a). For the temperature peak near the inlet, the onset of temperature rise and its maximum value are predicted accurately. For the temperature peak in the middle of the pipe, the onset of temperature increase is not captured accurately and the maximum temperature is overpredicted. For Onatskii-359, wall temperature reaches the pseudo-critical value approximately

in the middle of the pipe. Numerical simulation captures accurately the onset of heat transfer deterioration and the maximum value of temperature (see Figure 3b). However, the recovery of heat transfer near the exit of the pipe was not predicted by the model.

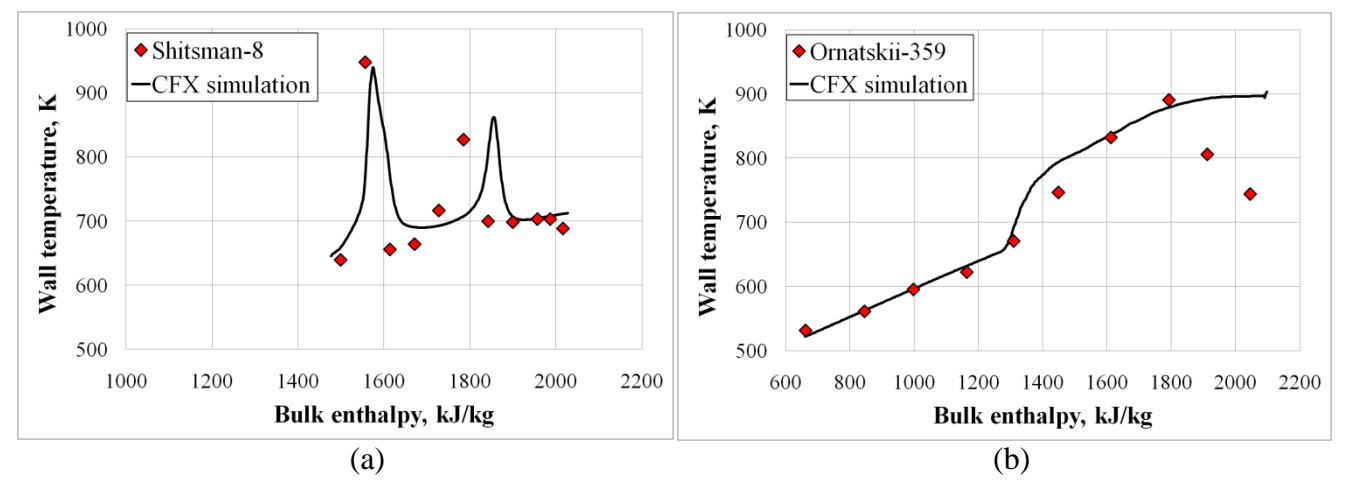


Figure 3 Axial temperature distribution as a function of bulk enthalpy for Shitsman-8 experiment (a), for Ornatskii-359 experiment (b).

As shown in Figure 4, radial velocity profiles significantly differ for the two considered experiments. Shitsman-8 experiment was performed for low values of mass flux for which the buoyancy force plays a dominant role in the process of heat transfer deterioration. Figure 4a shows that after heat transfer deterioration (L/D = 75 and 125) portion of fluid near the wall flows faster than in the centre of the pipe, forming m-shape. After recovery from heat transfer deterioration (L/D = 100), a flatten velocity profile is observed. Ornatskii-359 experiment was performed for a high mass flux. It was observed that with increasing values of mass flux the buoyancy effect diminishes. Figure 4b shows the velocity profiles typical for the turbulent flow and m-shape does not occur. After heat transfer deterioration (L/D = 200), flow accelerates.

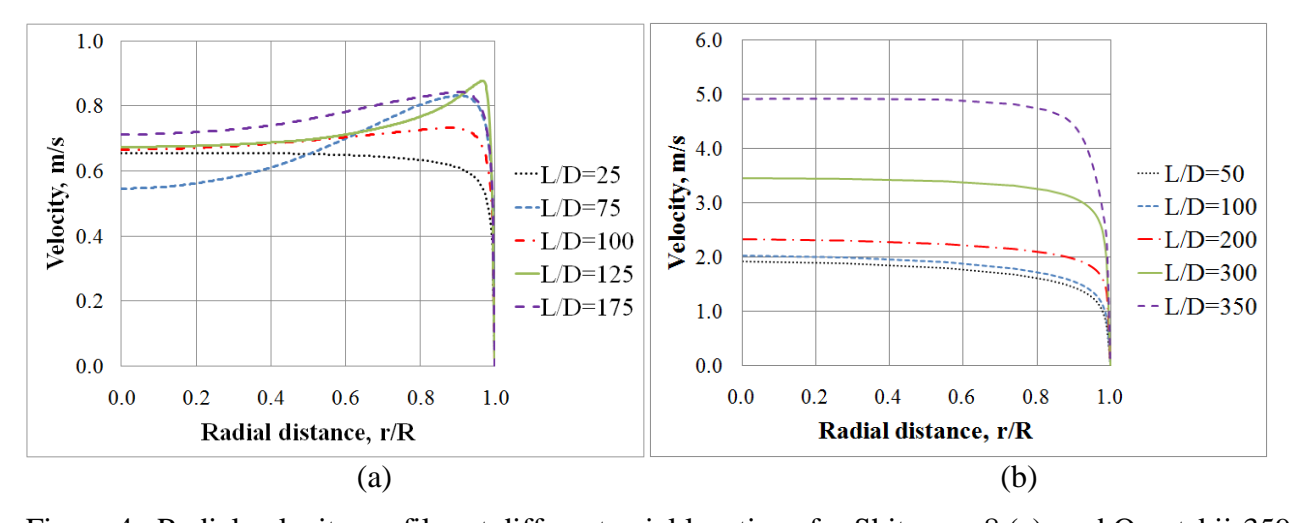


Figure 4 Radial velocity profiles at different axial locations for Shitsman-8 (a), and Ornatskii-359 (b).

Figure 5 shows radial distribution of density, dynamic viscosity, specific heat and thermal conductivity at different locations in the pipes for both experiments.

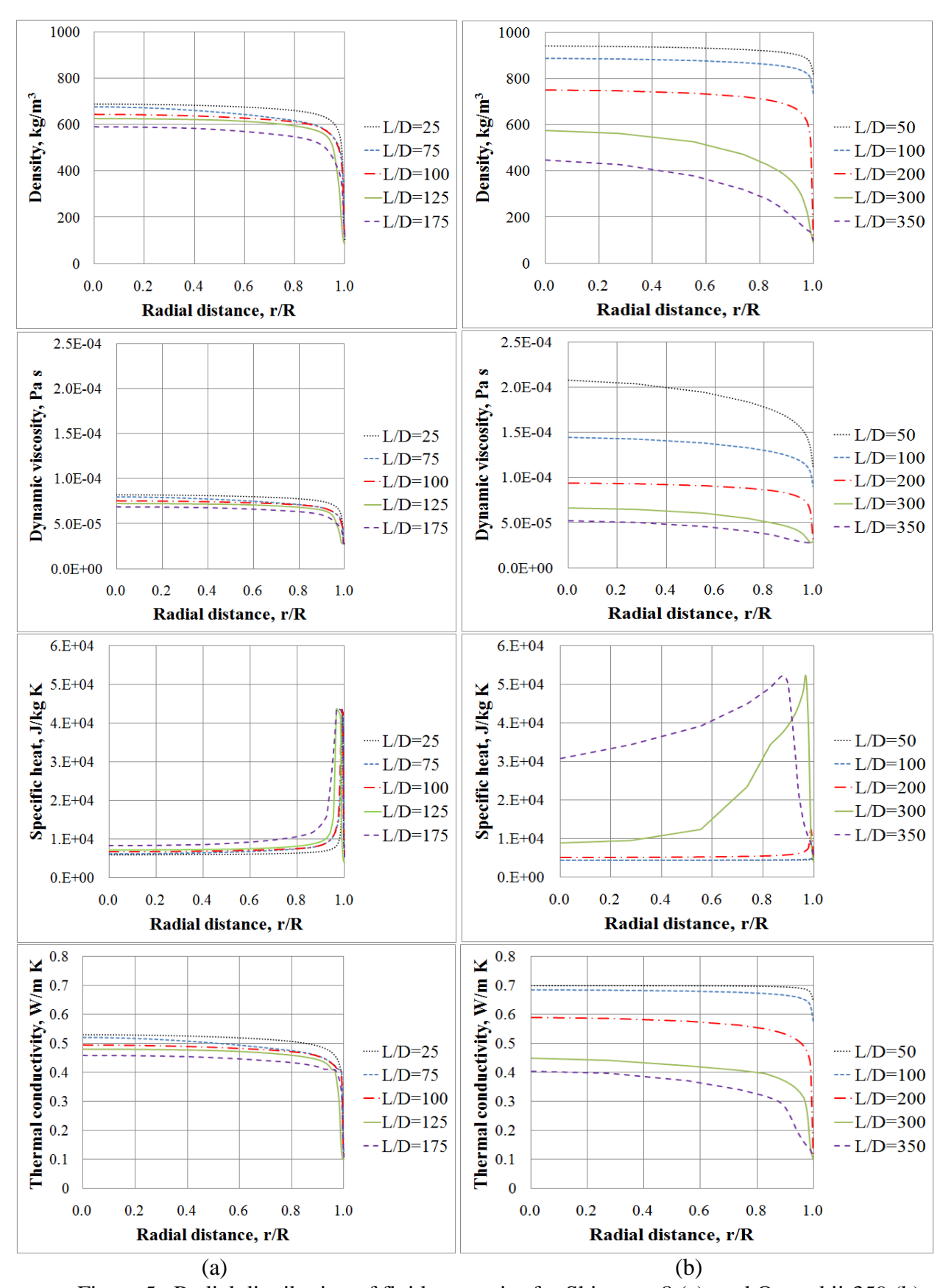


Figure 5 Radial distribution of fluid properties for Shitsman-8 (a), and Ornatskii-359 (b).

For the Ornatskii-359 experiment, properties vary significantly between inlet and outlet of the pipe (see Figure 5b), much more than for Shitsman-8 (see Figure 5a). Although the buoyancy effect in the phenomenon of heat transfer deterioration is negligible for high mass fluxes (Ornatski-359), decrease in heat transfer coefficient may be caused by significant change in thermal-physical properties [1].

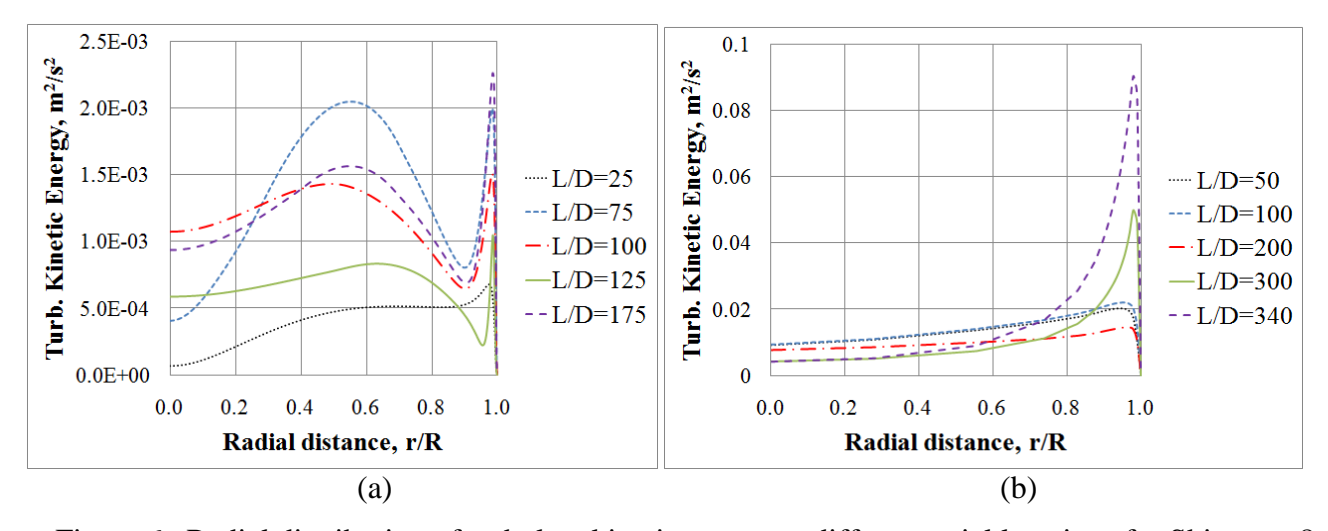


Figure 6 Radial distribution of turbulent kinetic energy at different axial locations for Shitsman-8 experiment (a), and for Ornatskii-359 experiment (b).

Figure 6 shows radial distribution of turbulence kinetic energy at different axial locations. Production of turbulence energy is proportional to a derivative of flow velocity. As shown in Figure 4a, the velocity profile takes the m-shape for Shitsman-8, therefore turbulence kinetic energy is produced not only near the wall, but also in the inner part of the tube (see Figure 6a). As shown in Figure 6b, turbulence kinetic energy is produced mainly in the near-wall region for the Ornatskii-359 experiment, due to the velocity profile.

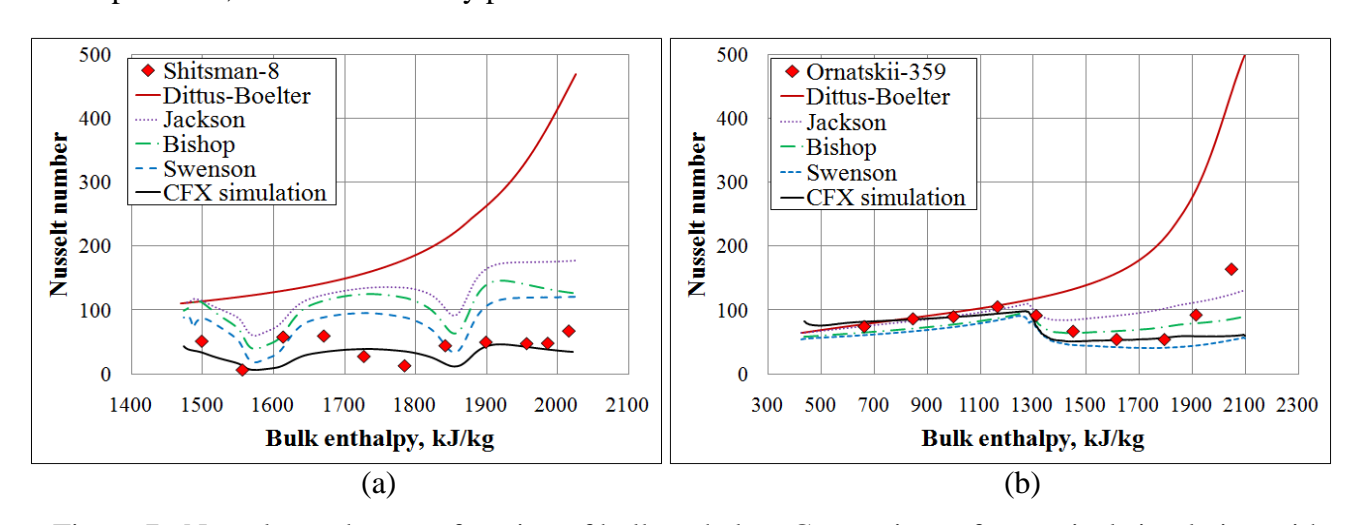


Figure 7 Nusselt number as a function of bulk enthalpy. Comparison of numerical simulation with Dittus-Boelter, Jackson, Bishop and Swenson correlations and with experimental data Shitsman-8 (a), and Ornatskii-359 (b).

Figure 7 shows plots of Nusselt number as a function of bulk enthalpy where results of numerical simulations are compared with empirical correlations and experiments. Definitions of all used correlations are given in the subsection 1.4. In the case of low mass and heat fluxes (Shitsman-8), CFX results are in a better agreement with experimental data than the correlation predictions. In the case of low mass and heat fluxes (Ornatskii-359), CFX results show good agreement with experimental data just as Swenson, Bishop and Jackson correlations.

2.1 Sensitivity analysis

The model sensitivities were examined on the mesh discretization, boundary conditions (inlet temperature, mass flux, heat flux and system pressure) and numerical parameters.

2.1.1 Space convergence

The space convergence is required to achieve the numerically accurate solution and mesh independence. It aims to eliminate any possible numerical influences introduced by the size of grid and its distributions. The grid refinement was performed by increasing the number of control volumes in the radial direction. As it was obtained from preliminary calculations, grid refinement in the axial direction does not influence results. The cell size of 3 mm in the axial direction was found sufficient to obtain a good resolution of temperature at the wall. As shown in Figure 8, numerical grid converged for 202 cells in the radial direction for Shitsman-8, and 50 cells in the radial direction for Ornatskii-359.

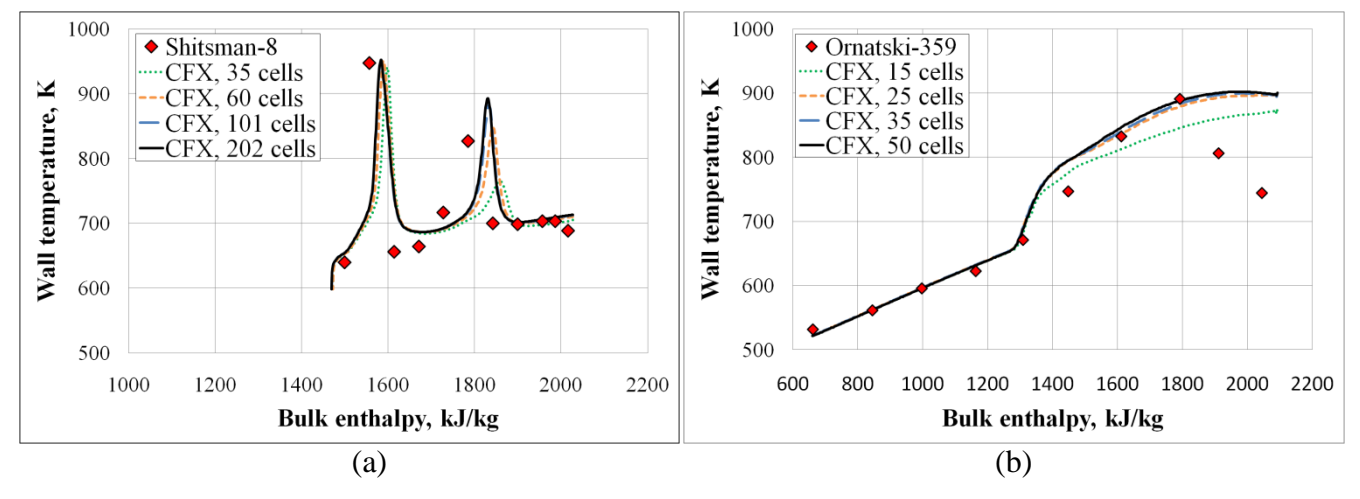


Figure 8 Grid convergence obtained for the axial temperature distribution by increasing the number of control volumes in the radial direction, for Shitsman-8 (a) and for Ornatskii-359 (b).

2.1.2 Operational conditions

The influence of uncertainties in boundary conditions on a prediction of the axial wall temperature was investigated. Estimated accuracies of the main process parameters are given in Table 2.

Quantity	Pressure	Mass flux	Heat flux	Inlet temperature
Accuracy	1.0%	1.0%	1.5%	2.0 K

Table 2 Estimated accuracy of main process parameters for the wall temperature measurements.

Results obtained from the numerical simulations of experiments Shitsma-8 and Ornatskii-359 (see Figure 3) are considered as base cases to carry out further calculations. The following variations were calculated for each experiment: inlet temperature ± 2 K, system pressure $\pm 1.0\%$, heat flux at the pipe wall $\pm 1.5\%$ and inlet mass flux $\pm 1.0\%$.

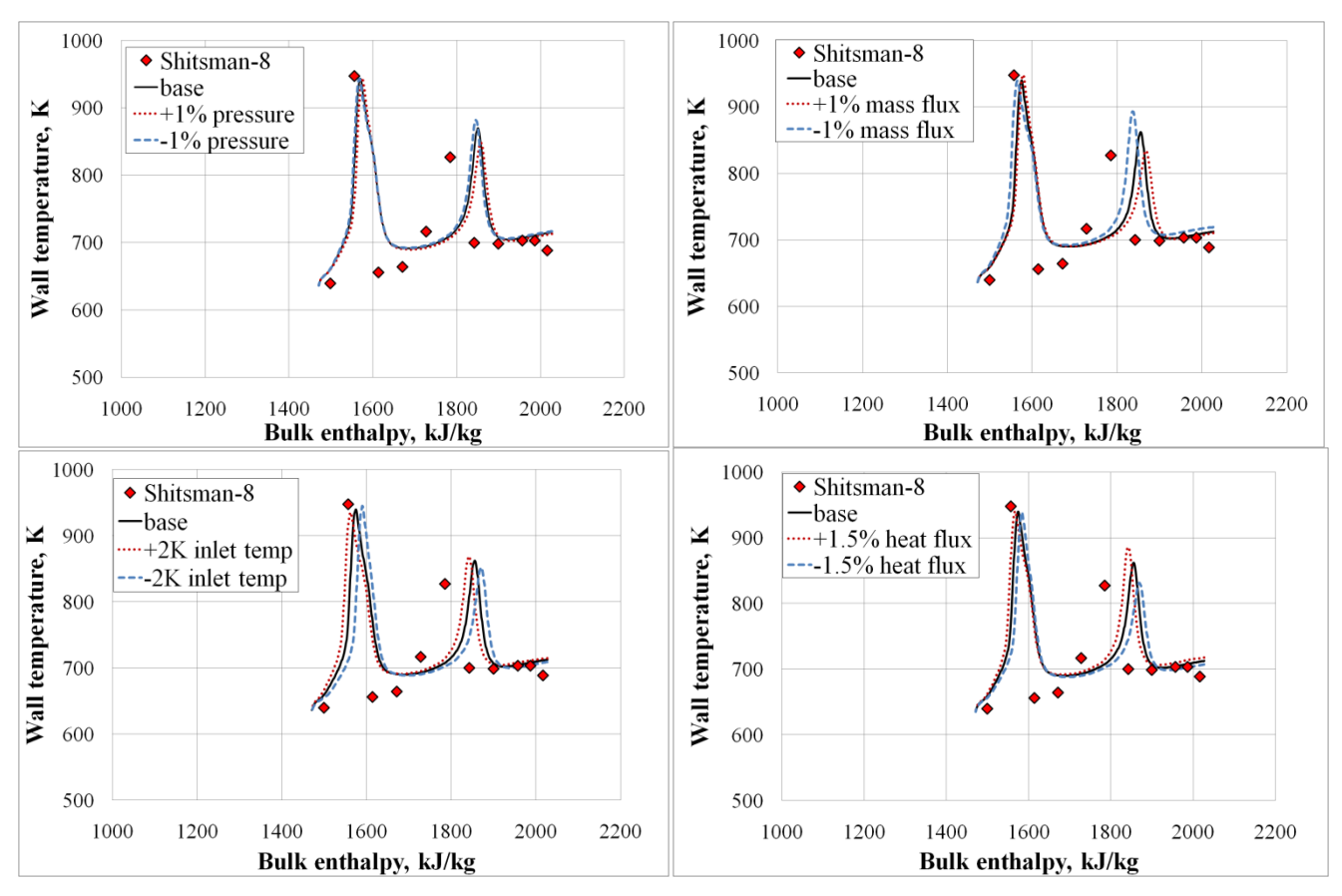


Figure 9 Sensitivity of wall temperature prediction to inlet temperature, system pressure, heat flux and inlet mass flux for Shitsman-8.

Figure 9 shows sensitivity of wall temperature prediction to inlet temperature, system pressure, heat flux and inlet mass flux for the Shitsman-8 experiment. The model shows low sensitivity to variation of the system pressure, medium sensitivity to variation in inlet temperature, and high sensitivity to changes of heat flux and mass flux. Increasing the heat flux at the wall leads to a higher wall temperature and sooner occurrence of heat transfer deterioration. While decreasing the heat flux, the temperature goes down and heat transfer deterioration appears later. For increased value of mass flux, cooling of the heated wall is intensified and wall temperature decreases. For decreased mass flux, cooling is worsened leading to increase of the wall temperature and sooner appearance of the heat transfer deterioration.

Figure 10 shows sensitivity of wall temperature prediction to inlet temperature, system pressure, heat flux and inlet mass flux for the Ornatskii-359 experiment. The model is not sensitive to variations in the system pressure and inlet temperature, and it shows medium sensitivity to changes of heat flux and mass flux. None of the changes in boundary conditions influenced prediction of the onset of heat transfer deterioration.

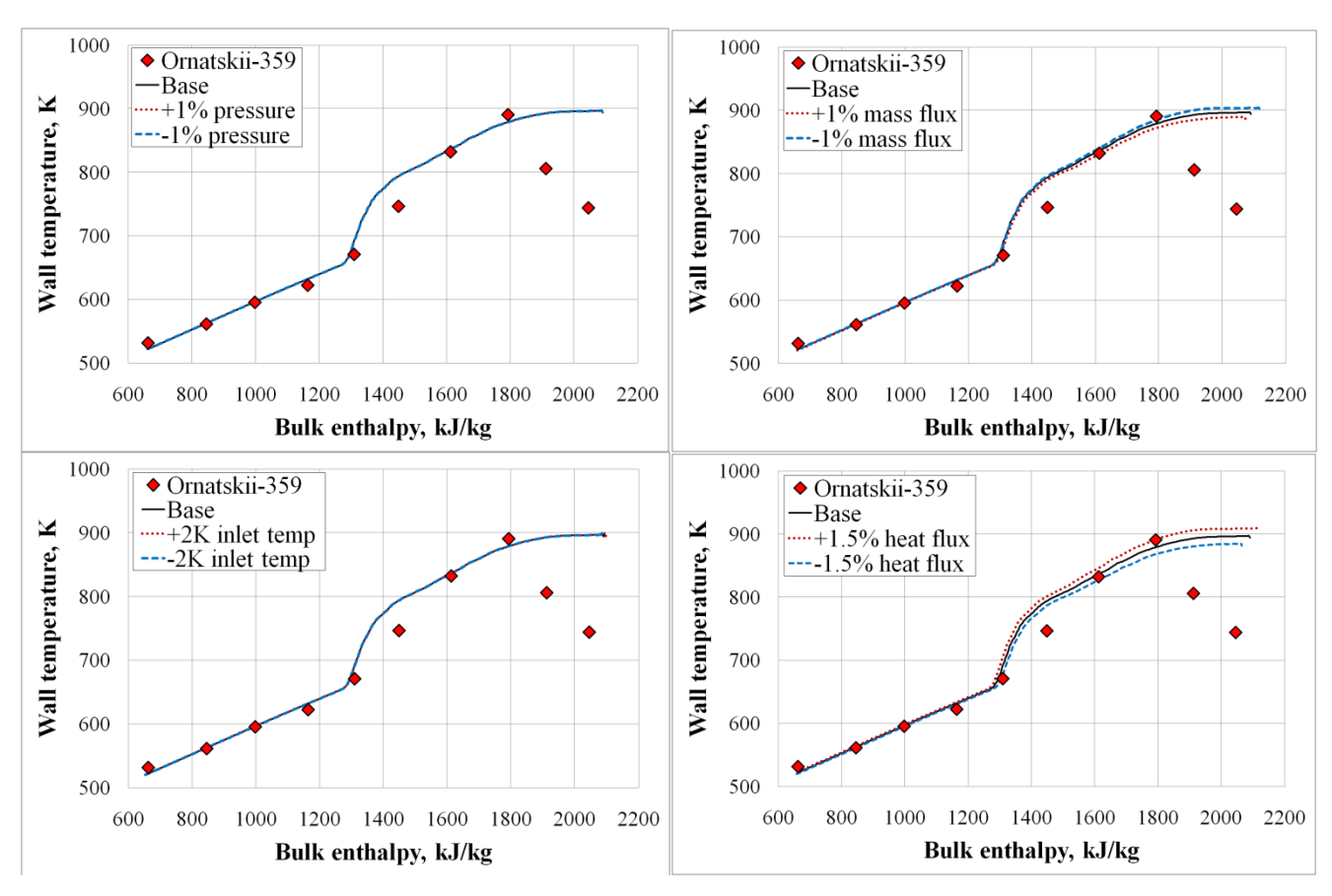


Figure 10 Sensitivity of wall temperature prediction to inlet temperature, system pressure, heat flux and inlet mass flux for Ornatskii-359.

3. Conclusions

The commercial CFD code ANSYS CFX 12.1 is used to simulate the heat transfer to water under supercritical conditions. Results were verified against two different experiments, Shitsman-8 performed at low mass and heat fluxes, and Ornatskii-359 performed at high mass and heat fluxes. Both are characterized by heat transfer deterioration. Simulations were also compared to selected empirical correlations for the Nusselt number.

In ANSYS CFX 12.1, implementation of water properties used in the numerical simulations was according to IAPWS IF97. It must be kept in mind that differences between the industrial formulation IAPWS-IF97 and the IAPWS-95 formulation cannot be neglected in the near vicinity of the critical point.

For Shitsman-8, both peaks in the axial temperature distribution are captured. Temperature peak near the inlet was predicted accurately. For Onatskii-359, numerical simulation captures accurately the onset of heat transfer deterioration and the maximum value of temperature, but without the recovery of heat transfer near the pipe exit.

For low values of mass flux (Shitsman-8), the buoyancy force plays a dominant role in the process of heat transfer deterioration. For high values of mass flux, the buoyancy effect diminishes and significant variation in properties leads to the phenomenon of heat transfer deterioration.

Empirical correlations for the Nusselt number by Swenson, Bishop and Jackson show much better agreement with experimental data for the Ornatskii-359 experiment than for the Shitsman-8 experiment.

Sensitivity study shows, for the Shitsman-8 experiment, low sensitivity to variation of the system pressure, medium sensitivity to variation in inlet temperature, and quite high sensitivity to changes of heat flux and mass flux. For Ornatskii-359, insignificant sensitivity to variation in the system pressure and inlet temperature, and medium sensitivity to changes of heat flux and mass flux.

4. Acknowledgements

The work described in this paper was partially funded by the FP7 European Commission Collaborative Project THINS No. 249337.

5. References

- [1] S. Koshizuka, N. Takano and Y. Oka, "Numerical analysis of deterioration phenomenon in heat transfer to supercritical water", Int. Journal of Heat and Mass Transfer, Vol. 38, No. 16, 1995, pp. 3077-3084
- [2] X. Cheng, T. Schulenberg, D. Bittermann and P.Rau, "Design analysis of core assembly for supercritical pressure conditions", Nuclear Engineering and Design, Vol. 223, No. 3, 2003, pp. 279-294
- [3] D.M. McEligot, J.D. Jackson, "'Deterioration' criteria for convective heat transfer in gas flow through non-circular ducts", Nuclear Engineering and Design, Vol. 232, No. 3, 2004, pp. 327-333
- [4] ANSYS, Inc, "ANSYS CFX Solver Theory Guide", Canonsburg, PA, USA, 2010
- [5] D. Palko and H. Anglart, "Theoretical and numerical study of heat transfer deterioration in High Performance Light Water Reactor", Science and Technology of Nuclear Installations, Vol. 2008, No. 405072
- [6] S. B. Pope, "Turbulent flows", Cambridge University Press, Cambridge, UK, 2000, p. 384
- [7] G. Brunner, "Near critical and supercritical water. Part I. Hydrolytic and hydrothermal processes", Journal of Supercritical Fluids, Vol. 47, No. 3, 2009, pp. 373-381.
- [8] I.L. Pioro and R.B. Duffey, "Experimental heat transfer in supercritical water flowing inside channels (survey)", Nuclear Engineering and Design, Vol. 235, No. 22, 2005, pp. 2407-2430.
- [9] J.D. Jackson and W.B. Hall, "Forced Convection Heat Transfer to Fluids at Supercritical Pressure Turbulent Forced Convection in Channels and Bundles", Hemisphere Publishing Corporation (1979) pp. 563–611.
- [10] J.D. Jackson and W.B. Hall, Influences of Buoyancy on Heat Transfer to Fluids Flowing in Vertical Tubes under Turbulent Conditions, Hemisphere Publishing Corporation (1979) pp. 613–640.
- [11] F.W. Dittus and L.M.K. Boelter, "University of California Publications in Engineering", Vol. 2, p.433, Berkeley, 1930.
- [12] I.L. Pioro, H.F. Khartabil, R.B. Duffey, "Heat transfer to supercritical fluids flowing in channels empirical correlations (survey)", Nuclear Engineering and Design, Vol. 230, No. 1-3, 2004, pp. 69-91.

- [13] S.I. Mokry, P.L. Kirillov, I.L. Pioro and Y.K. Gospodinov, "Supercritical water heat transfer in a vertical bare tube: normal, improved, and deteriorated regimes", Nuclear Technology, Vol. 172, No. 1, 2010, pp.60-70.
- [14] M.T. Kao, M. Lee, Y.M. Ferng and C.C. Chieng, "Heat transfer deterioration in a supercritical water channel", Nuclear Engineering and Design, Vol. 240, No. 10, 2010, pp. 3321-3328.
- [15] Q.L. Wen and H.Y. Gu, "Numerical simulation of the heat transfer deterioration phenomenon in supercritical water through vertical tube", Annals of Nuclear Energy, Vol. 37, 2010, pp. 1272-1280.
- [16] G.V. Alekseev, V.A. Silin, A.M. Smirnov and V.I. Subottin, "Study of the thermal conditions on the wall of a pipe during the removal of heat by water at a supercritical pressure", High Temp., Vol. 14, No. 4, 1979, pp. 683-687.
- [17] N.S. Kondratiev, "About regimes of the deteriorated heat transfer at flow of supercritical pressure water in tubes", Trans. IV All-Union Conf. Heat Transfer and Thermal-Hydraulics of Two-Phase Flow in Power Engineering Machines and Apparatuses, Leningrad, Russia, 1971, pp. 71-74.
- [18] A.P. Ornatskii, L.P. Glushchenko, E.T. Siomin, et al., "The research of temperature conditions of small diameter parallel tubes cooled by water under supercritical pressures", Proc. 4th Int. Heat Transfer Conf. Vol. VI, Paris, France, 1970.
- [19] V.S. Protopopov, I.V. Kuraeva and A.M. Antonov, "An approach to the determination of the condition of occurrence of deteriorated heat transfer regimes at supercritical pressures", High Temp., Vol. 11, No. 3, 1973, pp. 529-532.
- [20] V.S. Protopopov and V.A. Silin, "Approximate method of calculating the start of local deterioration of heat transfer at supercritical pressure", High Temp., Vol. 11, No. 2, 1973, pp. 399-401.
- [21] M.A. Styrikovich, T.K. Margulova and Z.L. Miropolskii, "Problems in the development of designs of supercritical boilers", Thermal Engineering, Vol. 14, No. 6, 1967, pp.5-9.
- [22] Y.V. Vikhrev, Y.D. Barulin and A.S. Konkov, "A study of heat transfer in vertical tubes at supercritical pressures", Thermal Engineering, Vol. 14, No. 9, 1967, pp.116-119.
- [23] W. Wagner et al., "The IAPWS Industrial Formulation 1997 for the Thermodynamic Properties of Water and Steam," ASME J. Eng. Gas Turbines and Power, Vol. 122, 2000, pp. 50-182.
- [24] W. Wagner and A. Pruss, "The IAPWS Formulation 1995 for the Thermodynamic Properties of Ordinary Water Substance for General and Scientific Use," *J. Phys. Chem. Ref. Data*, Vol. 31, 2002, pp. 387-535.
- [25] M.E. Shitsman, "Impairment of the heat transition at supercritical pressures", High Temperatures, Vol. 1, No. 2, 1963, pp. 237-244.
- [26] A.P. Ornatskii, L.F. Glushchenko and S.I. Kalachev, "Heat transfer with rising and falling flows of water in tubes of small diameter at supercritical pressures", Thermal Engineering, Vol. 18, No. 5, 1971, pp.137-141.
- [27] A.A. Bishop, R.O. Sandberg and L.S. Tong, "Forced convection heat transfer to water at near-critical temperatures and supercritical pressures", Report WCAP-2056, Part IV, November, Westinghouse Electric Corp., Pittsburgh, USA, 1964

The $14^{\rm th}$ International Topical Meeting on Nuclear Reactor Thermal-Hydraulics, NURETH-14 Toronto, Ontario, Canada, September 25-30, 2011

[28] H.S. Swenson, J.R. Carver, C.R. Karakala, "Heat transfer to supercritical water in smooth-bore tubes", Journal of Heat Transfer, Vol. 87, No. 4, 1965, pp. 477–484.